Title:

Lumbar corticospinal tract in rodents modulates sensory inputs but does not convey motor command

Authors:

Yunuen Moreno-Lopez[1], Charlotte Bichara[1], Philippe Isope, Matilde Cordero-Erausquin

[1]These authors contributed equally to this work

Affiliation (+ present address):

Institut des Neurosciences Cellulaires et Intégratives, CNRS UPR 3212, Université de Strasbourg

8 Allée du Général Rouvillois
67000 STRASBOURG
France

M.C.E. : https://orcid.org/0000-0002-1623-1773

P.I.: https://orcid.org/0000-0002-0630-5935

Y.M.L.'s present address: Burke Neurological Institute, White Plains, New York, NY 10605, United States

Corresponding Author :

Matilde Cordero-Erausquin
Tel: (+33) 3 88 45 66 60
Fax: (+33) 3 88 60 16 64
cordero@unistra.fr

Institut des Neurosciences Cellulaires et Intégratives - CNRS UPR 3212
8 allée du Général Rouvillois
67000 Strasbourg cedex, France

Classification : BIOLOGICAL SCIENCES / Neuroscience

Keywords : corticospinal, sensory gating, primary afferent depolarization, motor control

Abstract

It is generally assumed that the main function of the corticospinal tract (CST) is to convey motor commands to bulbar or spinal motoneurons. Yet the CST has also been shown to modulate sensory signals at their entry point in the spinal cord, through primary afferent depolarization (PAD). By sequentially investigating different routes of corticofugal pathways, we here demonstrate that motor and PAD commands in mice belong to segregated paths within the CST. PAD is carried out exclusively by the CST via a population of lumbar interneurons located in the deep dorsal horn. In contrast, the cortex conveys the motor command via a relay in the upper spinal cord or supraspinal motor centers. At lumbar level, the main role of the CST is thus the modulation of sensory inputs, which is an essential component of the selective tuning of sensory feedback, to ensure well-coordinated and skilled movement.

Impact statement

While the corticospinal tract is often considered exclusively as a motor path, we here demonstrate that, in the mouse lumbar cord, its main role is the modulation of sensory inputs.

Text

Introduction

Several brain and spinal structures have been involved in the generation and control of movement, in a task-depending manner. The cortex is classically associated to forelimb skilled movements (Starkey et al., 2005; Guo et al., 2015; Miri et al., 2017; Galinanes et al., 2018) and to complex locomotor tasks (obstacles crossing, leaning scale or beam, etc.) (Beloozerova and Sirota, 1993; DiGiovanna et al., 2016; Wang et al., 2017; Bieler et al., 2018) while its role in gross locomotion appears, if anything, minor (Beloozerova and Sirota, 1993; DiGiovanna et al., 2016). A coordinated movement relies not only on a proper motor command, but also on the online analysis of a constant multi-sensory feedback indicating whether the movement has reached the planned objective or requires correction (Akay et al., 2014; Fink et al., 2014; Azim and Seki, 2019). To optimize the analysis of the overwhelming quantity of reafferent information, the irrelevant (because expected) or redundant sensory inputs can be inhibited either at their entry point or further up along the sensory pathway, a phenomenon known as “sensory gating” (Seki and Fetz, 2012; McComas, 2016). Recent studies in mice have shown that presynaptic inhibition of proprioceptive feedback is essential for performing smooth movements in mice (Akay et al., 2014; Fink et al., 2014). Since the cortex has the ability to inhibit sensory information through primary afferent depolarization (PAD), this mechanism may underlie cortical sensory gating at the spinal level. Indeed, PAD can be evoked by the sensorimotor cortex in primates (Abdelmoumene et al., 1970), cats (Andersen et al., 1962; Carpenter et al., 1963; Andersen et al., 1964) and rats (Eguibar et al., 1994; Wall and Lidierth, 1997). Altogether, these data indicate the cortex can be involved in coordinated movements by modulating sensory afferent fibers via PAD, in addition to the classical drive of motoneurons. In this study, we aimed at elucidating the neuronal pathways conveying the cortical motor command and sensory control to the hindlimb in mice.

Whether for controlling motoneurons or modulating sensory information, the corticospinal tract (CST) is the most direct pathway to the spinal cord. Its involvement in motor control is long acknowledged, although its precise contribution might vary depending on the motor task (locomotion vs. skilled movement) or targeted limb (forelimb vs. hindlimb) (Miri et al., 2017; Wang et al., 2017; Karadimas et al., 2019). The CST has also been involved in cortically-evoked PAD in cats as a pyramidotomy abolishes it (Rudomin et al., 1986). However, discriminating sensory vs motor contribution has been hampered by the lack of proper tools to segregate functionally or anatomically overlapping paths.

Importantly, none of the CST functions can rely exclusively on direct CST contacts onto motoneurons (MN) as these represent the exception rather than the rule. Indeed, monosynaptic CST-MN contacts are present only in some higher primates, while CST-interneuronal connections are preponderant (in adults) across species (rodents and primates) (Alstermark et al., 2011; Ebbesen and Brecht, 2017; Ueno et al., 2018). In the recent years, specific genetic factors have enabled the identification of several interneuronal populations, and of their inputs, including those from the cortex (Hantman and Jessell, 2010; Bourane et al., 2015; Abraira et al., 2017; Ueno et al., 2018). In these populations, up to 65% of the neurons receive CST inputs (Ueno et al., 2018), but there is always a fraction of neurons that is not targeted by the CST. While manipulating these populations has been extremely informative to better understand their role, it remains unclear whether the observed functions can be specifically attributed to the targets of the CST or more generally to the complete population sharing identical genetic markers. Therefore, it is still difficult to assess the specific role of the targets of the CST in movements.

In this study, we have investigated the corticofugal paths conveying motor command and modulation of sensory inputs through PAD. We have in particular interrogated the contribution of the CST and its direct lumbar targets through the development of an innovative intersectional viral strategy. We show that cortically-evoked PAD in lumbar primary afferents is conveyed exclusively by the CST

through a population of lumbar interneurons. In contrast, our results suggest that motor command to the hindlimbs is relayed either through supraspinal motor centers, or through the CST with a propriospinal relay in the upper cord. The role of the lumbar CST thus appears to be mainly the modulation of sensory inputs, which in turn selectively increases sensory gain and refines motor control during movement.

Results

PAD and muscular contractions originates in the same cortical area

The rodent sensorimotor cortex has a highly somatotopic organization (Ayling et al., 2009). Mainly studied in a motor perspective, it has been repeatedly mapped for its ability to provoke motor contraction (Li and Waters, 1991; Ayling et al., 2009), but never for its ability to induce PAD. Cortically-evoked PAD may inhibit the transmission of sensory information from primary afferents to the central nervous system and can be experimentally assessed by recording dorsal root potentials (DRPs, Fig. 1A). We thus recorded DRPs *in vivo* in lumbar roots L4-L6 (conveying hindlimb sensory inputs) of Thy1::ChR2 mice, expressing channelrhodopsin2 in layer V cortical neurons (Arenkiel et al., 2007). DRP recordings were performed in isoflurane-anesthetized mice, and trains of photostimulations (5x 8 msec-pulses, 1 msec apart) were applied at different positions of the surface of the cortex according to a 500 µm-spaced grid. The area inducing the DRPs was centered at AP=-0.75 mm, L=1.5 mm (Fig. 1C, n=7 mice). On a different group of animals, electromyographic (EMG) recordings were performed in the tibialis anterior (*TA*) under ketamine/xylazine anesthesia (see Methods). The cortex was similarly mapped with trains of photostimulations (6x 1 msec-pulses, 2 msec apart) and the area inducing EMG was centered at : AP=-0.75 mm, L=1.75mm (n=5 mice; Fig. 1C).We observe that the two zones are

concentric, demonstrating that cortically-evoked PAD and motor command of the hindlimb can originate from the same cortical area.

Spinal targets of the CST

We next investigated the spinal circuit underlying cortically-evoked DRPs. DRPs can be segmentally-evoked by the activation of a neighboring root, dampening sensory inputs through GABA-dependent primary-afferent depolarization (Rudomin and Schmidt, 1999). GABAergic terminals presynaptic to proprioceptive fibers arise from GAD65 interneurons (Hughes et al., 2005; Betley et al., 2009) and their activation produces DRPs (Fink et al., 2014). We thus investigated whether the CST directly targets GAD65-expressing spinal lumbar neurons that could in turn lead to inhibition of primary afferents. In TdTomato-flex mice crossed with GAD65::GFP mice, we injected a monosynaptic anterograde transynaptic virus (AAV1-CBA::WGA-Cre) encoding the Cre-recombinase fused to the wheat germ agglutinin (WGA) (Libbrecht et al., 2017) in the area inducing hindlimb DRPs and EMG (Figure 1 – Figure Supplement 1). The fusion with WGA provides transynaptic properties to the Cre recombinase, which is then transferred to the cortex's monosynaptic targets where it triggers the expression of TdTomato (see Methods, Figure 1 - Figure Supplement 2). We evaluated the proportion of GAD65+ neurons among the spinal targets of the CST revealed by Td-Tomato expression (Fig. 1D-E): 16.4±3.2% of spinal Td-Tomato positive neurons were GAD65::GFP+ (69 neurons out of 427, n=3 mice), suggesting that the cortically-evoked DRP could be mediated directly by the activation of a GAD65+ spinal target of the CST. Cholinergic terminals are also known to be presynaptic to primary afferents (Ribeiro-da-Silva and Cuello, 1990; Pawlowski et al., 2013) and an alternative mechanism for segmental PAD involving cholinergic pathways has been proposed (Hochman et al., 2010). By performing a similar experiment in ChAT::EGFP mice, only 2.2±1.8% of the targets of the CST were ChAT::EGFP positive (1 out of 45 neurons, n=4 mice), excluding a direct involvement of a cholinergic mechanism (Figure 1 - Figure Supplement 3). The majority of CST targets in the spinal cord thus appear to be glutamatergic neurons.

113 *Segregation of pathways for cortically-evoked DRPs and EMGs*

114 Although lumbar DRPs and tibialis-EMGs (TA-EMGs) are elicited by the same area in the mouse
115 sensorimotor cortex, whether they share the same corticofugal pathway and spinal circuits remains
116 unknown. We first interrogated the contribution of indirect cortical-to-spinal pathways to these two
117 functions (Fig. 2). Since broad photostimulation of the cerebral cortex in Thy1::ChR2 activates an
118 heterogeneous population of layer V cortical neurons (Arenkiel et al., 2007) we selectively lesioned
119 the direct CST (Fig. 2B) using an acute electrolytic lesion at the level of the pyramidal decussation
120 (pyramidotomy) (Figure 2 - Figure Supplement 1A, C). This protocol spares CST collaterals targeting
121 brainstem motor nuclei that branch more rostrally (Akintunde and Buxton, 1992; Alstermark and
122 Pettersson, 2014) as well as rubrospinal or reticulospinal tracts that can be activated by direct
123 corticorubral or corticoreticular neurons (Fig. 2B). Cortically evoked DRPs were completely abolished
124 by this pyramidotomy (DRP amplitude before: 3.8 µV± 0.32 µV; after: 0.30 µV± 0.12 µV , n=3 mice,
125 p=0.006), whereas cortically-evoked EMGs were hardly affected (S/N Ratio 3.3± 0.61 before, 2.2 ± 0.1
126 after, n=4 mice, p=0.517, all Z-Scores above significance after lesion, Figure 2 - Figure Supplement 2B)
127 (Fig. 2C-D). This demonstrates that indirect cortical-to-spinal pathways (involving supraspinal motor
128 centers) do not encode cortically-evoked DRPs but have a major role for cortically-evoked motor
129 contraction of the hindlimb. These results show that, in rodents, the CST mediates cortically-evoked
130 DRPs and hence modulates sensory inputs in a presynaptic manner.

131 Although the contribution of the rubrospinal or reticulospinal tracts to motor command is well
132 acknowledged in both rodents and primates, the CST is also believed to encode motor command
133 (Wang et al., 2017). This could have been underrated by simultaneous stimulation of the indirect
134 cortical-to-spinal pathways in Thy1::ChR2 mice. We thus interrogated the specific contribution of the
135 CST to motor contraction by targeting exclusively these neurons through injection of a ChR2-encoding
136 retrograde virus (AAVrg-CAG-hChR2-H134R-tdTomato) in the lumbar spinal cord (Fig. 3A). As expected,
137 the infected corticospinal neurons were located in the area delimited by the previous functional

138 mapping of hindlimb muscle contraction and DRP (Fig. 3B-C). Photostimulation (at the cortical level)
139 induced a robust EMG signal (S/N Ratio 2.4±0.52, n=5 mice, Fig. 3E, upper), demonstrating that CS
140 neurons triggered motor contraction. Because some CS neurons send collaterals to supraspinal regions
141 involved in motor command (Akintunde and Buxton, 1992), we next addressed whether the motor
142 command traveled through the direct cortical-to-spinal branch of CS neurons or via supraspinal relays.
143 A caudal pyramidotomy (Figure 2 - Figure Supplement 1C) completely abolished the EMG signal evoked
144 by cortically activating CS neurons (S/N Ratio 0.9±0.12; n=3 mice, p=0.013; all Z scores below
145 significance after pyramidotomy, Figure 2 - Figure Supplement 2C) (Fig. 3D-E). This demonstrates that,
146 while supraspinal collaterals of the CST do not trigger motor output, direct spinal branches can drive
147 motor command. However, this contribution does not seem significant when other cortical neurons
148 are co-activated.

149 *Spinal targets of the CST evoke DRPs but not muscular contraction*

150 Because both DRPs and EMGs of a given limb are encoded by the same sensorimotor cortical area and
151 can be conveyed by the spinal branch of the CST, we next interrogated whether these functions are
152 segregated at the spinal level. CS neurons projecting to the lumbar spinal cord can give off collaterals
153 at the cervico-thoracic level (Kamiyama et al., 2015; Karadimas et al., 2019) and contact cervical
154 propriospinal neurons (Ueno et al., 2012; Ni et al., 2014) that in turn project to lumbar motoneurons
155 to relay motor command (Ni et al., 2014). Indeed, many experiments demonstrated that these neurons
156 are involved in segmental coordination (Miller et al., 1975; Nathan et al., 1996; Reed et al., 2006; Reed
157 et al., 2009). In order to test the contribution of the lumbar branch of CS neurons and rule out
158 antidromic stimulation of rostral collaterals, we combined the transynaptic tool used in Figure 1 with
159 an intersectional approach at the lumbar level. We first identified the lumbar segments containing CST
160 targets by using cortical injection of AAV1-CBA::WGA-Cre in TdTomato-flex mice (Fig. 4A): CST targets
161 were concentrated in spinal lumbar segments L2-L3, rostral to the large pools of motoneurons, in the
162 contralateral deep dorsal horn (laminae IV to VII) (Fig. 4B). CST targets were mostly located in the

163 medial zone, lateral to the dorsal funiculus, where CST fibers penetrate the grey matter. We thus
164 combined the cortical injection of AAV1-CBA::WGA-Cre with the spinal (L4) injection of an AAV (AAV9-
165 Ef1a-DIO-ChETA-EYFP) encoding for a Cre-dependent form of ChETA (a ChR2 variant (Gunaydin et al.,
166 2010)) (Fig. 4C). ChETA expression was therefore restricted to the lumbar targets of the CST (Fig. 4C,
167 D). Photostimulation of these neurons through the spinal surface induced DRPs in the ipsilateral
168 lumbar root of 8 out of 9 mice (2.93 ± 0.48 µV, n=8 mice, Fig. 4E-G), demonstrating that DRPs can be
169 directly controlled by the CST projecting to the lumbar cord through local interneurons. However,
170 photoactivation of these same lumbar targets of the CST failed to elicit hindlimb movements or muscle
171 contraction as attested by EMG recordings (S/N Ratio 1.0±0.02; n=7 mice, Z-Scores below significance,
172 Figure 2 - Figure Supplement 2D) (Fig. 4E-G). These results argue that CST-evoked motor command is
173 mediated by a spinal circuit located at another spinal level. Cortically-evoked DRPs and EMGs thus
174 follow a similar corticofugal pathway that segregates at the spinal level.

175

176 **Discussion**

177 In this study, we have evaluated the contribution of the CST to the cortical control of movements,
178 either through its ability to convey the muscle contraction command or to modulate sensory inputs.
179 We found that the modulation of sensory inputs from the hindlimb (DRP in lumbar sensory roots) is
180 exclusively carried out by the CST via a population of lumbar interneurons located in the deep dorsal
181 horn. In contrast, the cortex induces muscle contraction of the hindlimb (*TA*) through a relay in the
182 upper spinal cord or supraspinal motor centers. The two mechanisms are therefore segregated, and
183 the main role of the lumbar CST appears to be the modulation of sensory inputs.

184 *Reliability of circuit investigations*

185 We have identified the cortical area involved in these two mechanisms through functional means:
186 cortically-evoked DRPs and EMGs. For ethical and technical reasons, most of these recordings were

187 performed on different animals and conditions. First, EMG recordings after cortical stimulation
188 required a light anesthesia level (Tennant et al., 2011), only possible using Ketamine/Xylazine. Such a
189 light anesthesia is not ethically compatible with the large and invasive surgery required for recording
190 cortically-evoked DRPs. DRPs were thus recorded under isoflurane anesthesia under which no
191 cortically-evoked EMG could be recorded. We therefore acknowledged that the cortical zone
192 responsible for DRPs, smaller than the one responsible for EMGs, might have been underestimated
193 by the deeper anesthesia. We thus did not attempt to quantitatively compare EMG vs DRP map
194 extensions, but concluded that they partially overlap allowing us to stimulate at the center of two
195 maps.

196 Circuit investigation also rely on the efficiency of pyramidotomies which affect the spinal branch of
197 CS tract while sparing CST collaterals targeting brainstem motor nuclei, that are branching more
198 rostrally (Akintunde and Buxton, 1992). We performed similar pyramidotomies in two different
199 group of mice, either Thy1::ChR2 or ChR2-retro group (Fig. 1, Fig. 2, Fig. 1 - Figure Supplement 3). In
200 the latter group, in which only CST expressed ChR2, we observed a complete loss of cortically-evoked
201 EMGs after pyramidotomy. These results confirm that the pyramidotomy was efficient to block CST-
202 induced EMG. Therefore, the remaining EMG signal after pyramidotomy in Thy1::ChR2 mice is likely
203 the result of a non-CST pathway.

204 *Anatomical definition of the hindlimb sensorimotor cortex*

205 In our study, the cortical area inducing hindlimb contraction is similar to that previously reported in
206 mice (Li and Waters, 1991; Ayling et al., 2009). This cortical area (centered around 1mm caudal and
207 1,5mm lateral to bregma) spans over the motor cortex and but also partly over the primary
208 somatosensory cortex according to some atlases and studies (Kirkcaldie et al., 2012; Liu et al., 2018;
209 Karadimas et al., 2019). We thus use the conservative term “hindlimb sensorimotor cortex”.
210 Interestingly, we found that stimulation of this area also induced PAD at the lumbar level. This
211 overlap might be a specificity of the “hindlimb area” of the cortex (HLA), and may not generalize to

212 the “forelimb areas” (RFA and CFA). Indeed, the CS neurons from the forelimb areas are spatially
213 segregated (forming clusters projecting either to the dorsal or to the intermediate-ventral cervical
214 cord), while those from the HLA are largely intermingled (Olivares-Moreno et al., 2017). In addition,
215 our results demonstrate that the same cortical area is labelled after retrograde tracing from the
216 lumbar cord (Fig. 3C) excluding the existence of a different pool of cortico-lumbar neurons.

217 *Pathways conveying the cortical motor command*

218 Our study concludes that a large fraction of the cortical motor command to the hindlimb is conveyed
219 through non-CST pathways. These could involve the reticular formation or the red nucleus which
220 receive cortical innervation, project directly or indirectly onto spinal motoneurons, and control
221 different parameters of movements (Lavoie and Drew, 2002; Zelenin et al., 2010; Esposito et al.,
222 2014). Our recordings also suggest that the cortex conveys a motor command to the hindlimb
223 through the direct CST projecting to a different spinal segment as direct stimulation of the CS lumbar
224 targets failed to produce muscle contraction. The lack of muscle contraction cannot be attributed to
225 damages of spinal microcircuits due intraspinal AAV injection as none of the mice presented obvious
226 alteration in the behavior (e.g. locomotor, overt spontaneous pain behaviors) nor a long-lasting
227 weight loss. In addition, similar intraspinal injections were performed for the ChR2-retrograde group,
228 and in these animals, EMG was systematically observed after cortical stimulation, demonstrating the
229 integrity of required spinal circuits. Importantly, the optic fiber positioned at the surface of the cord
230 evoked an intraspinal LFP as deep as 1150 µm (data not shown), excluding the possibility that the
231 lack of muscle contraction is due to failure in the activation of CS-postsynaptic neurons.

232 We cannot rule out that some lumbar targets of the CST contribute to conveying the cortical motor
233 command to the hindlimb but were not labeled in large enough quantities through our transynaptic
234 approach. The efficiency of WGA-Cre transynaptic tracing might be target specific (Libbrecht et al.,
235 2017), and the number of labelled neurons in the spinal cord suggest that not all targets were
236 labeled. However, this would still implicate that these neurons are distinct from the ones implicated

237 in the generation of a DRP, and that these two functions use segregated lumbar pathways. While
238 these technical issues cannot be excluded, the recent report by Karadimas and collaborators
239 (Karadimas et al., 2019) strongly supports the hypothesis that the motor cortical command conveyed
240 by the CST relays in rostral spinal segments. Indeed, they demonstrate that the cortical motor
241 command to the hindlimb can be mediated by corticospinal neurons projecting to the cervical cord,
242 and then relayed by cervical-to-lumbar propriospinal neurons (Karadimas et al., 2019). Although we
243 selectively study CS projecting at least to the lumbar cord (through lumbar retrograde infection),
244 many CS neurons have collaterals at different spinal segments (Kamiyama et al., 2015). Therefore,
245 their photostimulation at the cortex level would activate cervical pathways in addition to lumbar
246 ones.

247 *Pathways conveying the cortical sensory control*

248 Beyond inducing hindlimb muscle contraction, we have characterized the ability of the cortex to
249 induce DRPs. DRPs are a measure of primary afferent depolarization (PAD), a phenomenon initially
250 described after stimulation of a neighboring afferent fiber (segmental PAD) (Wall and Lidierth, 1997).
251 Segmental PAD is mainly mediated by GABA-A receptors whose activation induces a depolarization
252 (due to a high chloride content of primary afferents) that reduces the amplitude of incoming action
253 potentials and thus inhibits synaptic transmission (Prescott and De Koninck, 2003; Doyon et al.,
254 2011). It has been proposed that the presynaptic GABAergic last order neuron, located in laminae V-
255 VI, is under the control of a first order excitatory interneuron which receives peripheral and
256 descending (including cortical) inputs (Eccles et al., 1962; Rudomin and Schmidt, 1999). Most last-
257 order GABAergic neurons express GAD65 (found in 90% of axo-axonic synapses onto primary afferent
258 terminals contacting motoneurons) (Betley et al., 2009). The targets of the CST identified by our
259 transynaptic labeling are indeed predominantly located in laminae IV-VI, and include a small
260 population of GAD65-expressing neurons. They represent a potential substrate for Cx-DRP that
261 would thus not require a spinal first order excitatory interneuron.

262 The control of incoming sensory information through PAD plays an important role in the generation
263 of coordinated movements and processing of sensory information, including nociceptive information
264 (McComas, 2016). GAD65-expressing neurons are essential for smoothed movements (Fink et al.,
265 2014), but whether they require peripheral or cortical information to do so is yet unknown. Similarly,
266 recordings in primates demonstrated that sensory information is inhibited in a modality- and phase-
267 dependent manner during voluntary movements (Seki et al., 2003, 2009; Seki and Fetz, 2012)
268 suggesting that this inhibition is somehow related to the motor command, but the exact underlying
269 mechanism remains to be elucidated. Here, we demonstrate that CS neurons from the same
270 sensorimotor cortex area (but not necessarily a single population) are able to relay both motor
271 command and sensory modulation to hindlimb, but through segregated pathways. By performing
272 recordings in anesthetized animals, and of the dorsal root that contains a variety of sensory
273 afferents, important questions remain unanswered. Future studies will need to elucidate the timing
274 and specificity of the sensory control we have described.

275

276 *Conclusion*

277 Altogether, our results demonstrate a segregation of pathways involved in cortically-evoked sensory
278 modulation vs. motor control. The direct corticospinal tract is able to induce motor contraction,
279 independently of its supraspinal collaterals, through spinal targets possibly located at the cervico-
280 thoracic level. However, we show that motor command is largely mediated by non-CST pathways,
281 most likely cortico-rubral, or -reticular ones. On the other hand, the major and essential role of the
282 lumbar rodent CST appears to be hindlimb sensory modulation at the primary afferent level, through
283 a population of lumbar target neurons whose activation is sufficient to produce DRPs. While the CST
284 has long been known to have different functions and to have progressively evolved towards an
285 essentially fine motor tract (Lemon, 2008), we here show that its prominent role in the rodent
286 lumbar cord is modulation of sensory inputs. This also forces re-interpretation of previous studies

287 aiming at promoting CST function in a therapeutic perspective, whether in mouse models of spinal
288 injury or neurodegenerative diseases such as amyotrophic lateral sclerosis. While most of these
289 studies have exclusively considered motor command aspects, our results provide a new perspective
290 to analyze these efforts by considering the primary role of rodent lumbar CST, i.e. sensory
291 modulation.

292

MATERIALS AND METHODS

Animal models. This study was carried out in strict accordance with the national and international laws for laboratory animal welfare and experimentation and was approved in advance by the Ethics Committee of Strasbourg (CREMEAS; CEEA35; agreement number/reference protocol: APAFIS# 12982 - 2017122217349941 v3). The following mice strains were used (adult males and females): Thy1::ChR2 (Cg-Tg(Thy1-COP4/EYFP)18Gfng/J, Jackson Laboratory), TdTomato-Flex (*Gt(ROSA)26Sor*$^{tm14(CAG\text{-}tdTomato)Hze}$/J, Jackson Laboratory), ChAT::EGFP(von Engelhardt et al., 2007), GAD65::GFP(Lopez-Bendito et al., 2004). All lines except GAD65::GFP were back-crossed (at least 10 generations) on a CD1 background. GAD65::GFP were on a C57Bl6/J background. The mice were housed in the Chronobiotron facility (UMS3415, CNRS, University of Strasbourg) in accordance with the European convention 2010/63/EU on the protection of animals used for scientific purposes.

Electrophysiological recordings.

EMG recording: Ketamine/Xylazine anesthesia was chosen to minimally affect muscular tone. After the initial anesthesia (150 mg/kg of ketamine, Imalgene 1000 and 10 mg/kg of Xylazine, Rompun 20%), complementary doses of Ketamine were given when the animal was showing signs of awakening (additional doses bridged by short exposure to Isoflurane 1–1.5%)(Tennant et al., 2011). Concentric EMG needle electrodes (Myoline Xp) were inserted in the *tibialis anterior (TA)* muscle of the animals and a ground electrode was inserted in the tail. Responses were collected with a recording amplifier (IR183A, Cygnus technology) in series with a second amplifier (Brownlee Precision, model440). The traces were filtered with a bandwidth of 0.1 Hz–10 kHz, recorded with Spike 2 software (version 8.00, CED, Cambridge, UK), and analyzed off line with Clampfit (pCLAMP, version 10.7) and home-made python routines (WinPython 2.7.10, Python Software Fundation). EMG responses were recorded after cortical or spinal photostimulation (see below), and the response to 3 consecutive stimulations was averaged for analysis. The area under the curve of the rectified average trace was calculated in a

318 window of 30ms, either 40 ms before (baseline noise, N) or 10 ms after (signal, S) the onset of the
319 stimulation. The EMG response was presented as the S/N ratio. In CST lesion experiments, all S/N ratios
320 were expressed as a % of the control S/N (average of 3 responses before the lesion). The noise level
321 (S/N of 1) was similarly expressed as a % of the above defined control S/N.
322 *DRP recording:* Under isofluorane (1.5-2%) anesthesia, the mice spinal cord was fixed with the spinal
323 cord unit of a stereotaxic frame (Narishige instruments). A laminectomy was performed to expose the
324 surface of lumbar L3-L6 spinal cord segments. A dorsal root (L4-L6) was dissected, cut before the DRG,
325 and a rootlet was suctioned with a glass pipet (sometime two rootlets were suctioned together). An
326 agar pool was created on the exposed spinal cord and filled with NaCl 0.9%. The
327 amplifiers/filters/software used were the same as for the EMG recordings. DRPs in response to 60
328 successive cortical or spinal photostimulations (see below) were averaged for analysis. The amplitude
329 of the response from the onset to the peak was measured using Clampfit 10.0. The amplitude of the
330 noise was similarly measured on a window preceding photostimulation. For spinal photostimulation,
331 DRPs and EMGs recordings of 3 series of photostimulation were averaged.
332 For electrophysiological recordings, we excluded animals that had a constant decreasing signals (run-
333 down) in otherwise stable conditions. For DRP recordings that required a delicate surgery, animals
334 were excluded from the study if the surgery was considered failed or if recovery and scaring processes
335 (after intraspinal AAV injection) were abnormal.
336
337 **Cortical photostimulation.** Optogenetic stimulation of the cortex was performed on anesthetized
338 animals while recording EMG or DRP. For the cortex, a craniotomy of approximately 9mm^2 was
339 performed under stereo microscope on the contralateral side from the recording site. Muscle
340 contraction, measured by EMG, was evoked by photostimulation with a 250 µm-probe (473 nm laser
341 source PSU-III-FDA) using the following protocol: trains of 6 pulses, 1 ms duration, 2 ms interval; 15 s
342 minimum between each train. DRPs were elicited by photostimulation with a 105 µm-probe (460 nm
343 LED source, Prizmatix) using the following protocol: trains of 5 pulses of 8 ms, 1 ms interval and 2 s

344 between each train. In both cases, the probe was moved at the surface of the cortex along a 500 µm-
345 spaced grid. Isopotential contour plots were created, using for EMGs the S/N and for DRPs the peak
346 amplitude (both normalized to the largest values in each animal) at each photostimulation point in the
347 cortex, using a linear interpolation on a set of X, Y, Z triples of a matrix. For EMG, only S/N ratio above
348 significance (Z-Score>3, Figure 2 - Figure Supplement 2A) were considered for the analysis. Then the
349 isopotentials contours were superimposed on the metric planes of the top view of the cortex(Kirkcaldie
350 et al., 2012).
351
352 **Spinal cord photostimulation.** Optogenetic stimulation of the spinal cord was performed on
353 anesthetized mice after laminectomy (described above for DRPs recordings), using a 1,1 mm probe
354 (LED source) first placed on the surface of the lumbar spinal cord (on top of the injection site). The
355 stimulation trains were those used for cortical stimulation. If no signal was observed when stimulating
356 on top of the injection site, the optical fiber was then swept rostrally and caudally on top the whole
357 lumbar segment, in order to try and obtain a signal. EMG and DRP recordings were sequentially
358 performed and required to alternate between different types of anesthesia: isoflurane (craniotomy
359 and laminectomy surgery), ketamine/xylazine (EMG recording), isoflurane 1.5–2 % (DRPs recordings).
360 Only the mice filling the two following criteria were kept for analysis: (i) TdTomato^{+}/EYFP^{+} neurons
361 were found in the stimulated area; (ii) the response was not limited to the stimulation window
362 (probable photoelectric artefact).
363
364 **Pyramidotomy.** Electrolytic lesion of the CST was performed in a subset of THY1::ChR2 and ChR2
365 retrogradely labeled mice, with 200 ms pulses, 30 mA using a constant current stimulator (Digitimer
366 Ltd thorug) through a silver bipolar electrode inserted in the pyramidal decussation (3.5-4 mm caudal
367 to Bregma, 6 mm deep). The brain was removed for histological analysis at the end of the experiment.
368
369 **Cortical and spinal injections.**

370 Brain injections (1.5–2 mm lateral, 0.5–1 mm caudal to Bregma, 0.5 mm deep) were performed as
371 previously described(Cetin et al., 2006) under isoflurane anesthesia (2–3%). Briefly, 90 to 270 nL of
372 virus was injected by manual pressure using a 5 mL syringe coupled to a calibrated glass capillary, under
373 visual control. Spinal injections were performed using a similar manual pressure protocol. The pipette
374 was inserted in the exposed space between two vertebrae (T13-L1, corresponding to spinal L4), as
375 previously described (Tappe et al., 2006). 0.45 µL of virus was injected 300 µm lateral to the midline
376 and 300-400 µm deep. In both cases, Manitol 12.5% was injected i.p. (0.2 – 0.5 ml) after the surgery
377 to enhance vector spread and improve transduction (Tjolsen et al., 1992). After spinal injection,
378 transfected neurons were found on multiple segments centered in L4 (depending on the animals, up
379 to the whole lumbar enlargement).
380 The animals were kept 2 weeks for the retroAAV injections and a minimum 5 weeks for dual injections
381 before in vivo DRPs and/or EMGs recordings or histological analysis. Animals for which post hoc
382 histological analysis demonstrated inappropriate injections coordinates were excluded from the
383 analysis.
384
385 **Viruses.** AAV2/1-CBA-WGA-CRE-WPRE was purchased at the molecular tools platform at the Centre de
386 recherche CERVO (Québec, Canada), and was used at a titer of $8x10^{12}$ vg/ml. AAV-Ef1a-DIO ChETA-
387 EYFP was a gift from Karl Deisseroth (Gunaydin et al., 2010) (Addgene viral prep # 26968-AAV9;
388 http://n2t.net/addgene:26968 ; RRID:Addgene_26968) and was used at a titer of 1×10^{13} vg/mL. AAV-
389 CAG-hChR2-H134R-tdTomato was a gift from Karel Svoboda (Mao et al., 2011) (Addgene viral prep #
390 28017-AAVrg; http://n2t.net/addgene:28017 ; RRID:Addgene_28017), and was used at a titer of
391 7×10^{12} vg/mL.
392
393 **Histology**
394 Mice were transcardially perfused with PB followed by 4% paraformaldehyde (PFA) in PB 0.1M, or, if
395 histological analysis followed electrophysiological recordings, the brain and spinal cord were post-fixed

396 overnight in PFA 4% in PB 0.1M. Serial 50 µm brain (coronal or sagittal) and spinal (transverse or
397 sagittal) sections were performed on a vibratome (Leica VT1000 S) and mounted using a DAPI staining
398 mounting medium (Vectashield, Vector laboratories).
399
400 **Image analysis.** The extent of the cortical injection site was estimated by measuring the spread of
401 reporter protein fluorescence (TdTomato) in the layer V of the cortex. The intensity of fluorescence
402 was analyzed as previously described(Lorenzo et al., 2008; Mesnage et al., 2011) on evenly spaced (250
403 µm apart) transverse brain sections imaged with a microscope (Axio Imager 2, Zeiss). Briefly, the "Plot
404 Profile" function of ImageJ software (W. Rasband, National Institutes of Health) was used to measure
405 the intensity of fluorescence along the horizontal axis of a 6000x250 µm rectangle containing the layer
406 V of the cortex (Figure 1 - Figure Supplement 1). These values were normalized to the highest intensity
407 for each animal, and used to plot a density map of each injection site. The contour of the injection area
408 was defined as 30% of the maximal intensity, corresponding to the approximate intensity of individual
409 neurons.
410 *Spatial distribution of corticospinal post-synaptic neurons:* Spinal_lumbar sections (50µm) were
411 mounted serially and imaged using a Zeiss epifluorescence microscope or a Leica SP5 II confocal
412 microscope. Images were aligned manually with Photoshop using the central canal and the dorsal
413 funiculus as landmarks. Each labeled neuron was assigned coordinates corresponding to its distance
414 to the center of the central canal (X and Y) and the index of the slice containing it (Z). This was used to
415 calculate the number of labeled neurons every 100 µm x 100 µm bins (XxY) (or 200 µm x200 µm X x Z)
416 in order to build density plots. The neuronal distribution was plotted using the "spline 16" interpolation
417 method of the matplotlib library in a homemade python script.
418
419 **Quantification and statistical analysis**. No prior sample size calculation was performed. The mean and
420 standard deviation of the Noise were measured from the 3 Noise values obtained from each EMG

recording, and used to calculate the Z-scores. The Z-score of each EMG response to the stimulation was calculated using the following equation:

$$\text{Z-score} = \frac{\text{Signal- mean Noise}}{\text{standard deviation of Noise}}$$

A Z-score of 1.96 or 3 corresponding to a significance level of 0.05 or 0.001 was chosen to discriminate significant responses from non-significant ones. The conservative choice of threshold was chosen in agreement with visual inspection of the traces, to ensure that any EMG responses was not simply due to noise. For each tests, the normality and variance equality were verified by SigmaPlot (Version 13, Copyright © 2014 Systat Softwara, Inc) using Shapiro-Wilk and Brown-Forsythe's methods, before we applied the parametric tests. All the data were analyzed using a one-way ANOVA and a post-hoc test was performed only if an effect showed statistical significance. The P-values for multiple comparison were measured using Holm-Sidak's method. Error bars in all Figures represent mean ± s.e.m., *$P < 0.05$, NS, no statistical significance ($P \geq 0.05$). The power of the tests was systematically attested to be above the desired power of 0.80.

Acknowledgments

We gratefully acknowledge the support from the CNRS and Strasbourg University; University of Strasbourg Institute for Advanced Study (USIAS) and ANR- 13-JSV4-0003-01 grants to MCE; ANR - 15-CE37-0001-01 CeMod, ANR - 19-CE37-0007-03 MultiMod, and ANR - 19-CE16-0019-01 NetOnTime to PI. YML was supported by a postdoctoral fellowhips from the Fondation pour la Recherche Médicale (SPF20160936264) and CB was funded by a fellowship from the Ministère de la Recherche. We also thank the following for providing/generating specific mouse lines: Gábor Szabó for GAD65::GFP, Jakob von Engelhardt for ChAT::EGFP. We thank Dr. Sophie Reibel-Foisset and the staff of the animal

facility (Chronobiotron, UMS 3415 CNRS and Strasbourg University) for technical assistance. We also thank Yves De Koninck, Frédéric Doussau and Didier Desaintjan for critical reading of the manuscript.

References

Abdelmoumene M, Besson JM, Aleonard P (1970) Cortical areas exerting presynaptic inhibitory action on the spinal cord in cat and monkey. Brain Res 20:327-329.

Abraira VE et al. (2017) The Cellular and Synaptic Architecture of the Mechanosensory Dorsal Horn. Cell 168:295-310 e219.

Akay T, Tourtellotte WG, Arber S, Jessell TM (2014) Degradation of mouse locomotor pattern in the absence of proprioceptive sensory feedback. Proc Natl Acad Sci U S A 111:16877-16882.

Akintunde A, Buxton DF (1992) Origins and collateralization of corticospinal, corticopontine, corticorubral and corticostriatal tracts: a multiple retrograde fluorescent tracing study. Brain Res 586:208-218.

Alstermark B, Pettersson LG (2014) Skilled reaching and grasping in the rat: lacking effect of corticospinal lesion. Front Neurol 5:103.

Alstermark B, Pettersson LG, Nishimura Y, Yoshino-Saito K, Tsuboi F, Takahashi M, Isa T (2011) Motor command for precision grip in the macaque monkey can be mediated by spinal interneurons. J Neurophysiol 106:122-126.

Andersen P, Eccles JC, Sears TA (1962) Presynaptic inhibitory action of cerebral cortex on the spinal cord. Nature 194:740-741.

Andersen P, Eccles JC, Sears TA (1964) Cortically Evoked Depolarization of Primary Afferent Fibers in the Spinal Cord. J Neurophysiol 27:63-77.

Arenkiel BR, Peca J, Davison IG, Feliciano C, Deisseroth K, Augustine GJ, Ehlers MD, Feng G (2007) In vivo light-induced activation of neural circuitry in transgenic mice expressing channelrhodopsin-2. Neuron 54:205-218.

Ayling OG, Harrison TC, Boyd JD, Goroshkov A, Murphy TH (2009) Automated light-based mapping of motor cortex by photoactivation of channelrhodopsin-2 transgenic mice. Nat Methods 6:219-224.

472 Azim E, Seki K (2019) Gain control in the sensorimotor system. Curr Opin Physiol 8:177-187.
473 Beloozerova IN, Sirota MG (1993) The role of the motor cortex in the control of accuracy of
474 locomotor movements in the cat. J Physiol 461:1-25.
475 Betley JN, Wright CV, Kawaguchi Y, Erdelyi F, Szabo G, Jessell TM, Kaltschmidt JA (2009) Stringent
476 specificity in the construction of a GABAergic presynaptic inhibitory circuit. Cell 139:161-174.
477 Bieler L, Grassner L, Zaunmair P, Kreutzer C, Lampe L, Trinka E, Marschallinger J, Aigner L, Couillard-
478 Despres S (2018) Motor deficits following dorsal corticospinal tract transection in rats:
479 voluntary versus skilled locomotion readouts. Heliyon 4:e00540.
480 Bourane S, Grossmann KS, Britz O, Dalet A, Del Barrio MG, Stam FJ, Garcia-Campmany L, Koch S,
481 Goulding M (2015) Identification of a spinal circuit for light touch and fine motor control. Cell
482 160:503-515.
483 Carpenter D, Lundberg A, Norrsell U (1963) Primary Afferent Depolarization Evoked from the
484 Sensorimotor Cortex. Acta Physiol Scand 59:126-142.
485 Cetin A, Komai S, Eliava M, Seeburg PH, Osten P (2006) Stereotaxic gene delivery in the rodent brain.
486 Nat Protoc 1:3166-3173.
487 Confais J, Kim G, Tomatsu S, Takei T, Seki K (2017) Nerve-Specific Input Modulation to Spinal Neurons
488 during a Motor Task in the Monkey. J Neurosci 37:2612-2626.
489 DiGiovanna J, Dominici N, Friedli L, Rigosa J, Duis S, Kreider J, Beauparlant J, van den Brand R,
490 Schieppati M, Micera S, Courtine G (2016) Engagement of the Rat Hindlimb Motor Cortex
491 across Natural Locomotor Behaviors. J Neurosci 36:10440-10455.
492 Doyon N, Prescott SA, Castonguay A, Godin AG, Kroger H, De Koninck Y (2011) Efficacy of synaptic
493 inhibition depends on multiple, dynamically interacting mechanisms implicated in chloride
494 homeostasis. PLoS Comput Biol 7:e1002149.
495 Ebbesen CL, Brecht M (2017) Motor cortex - to act or not to act? Nat Rev Neurosci 18:694-705.
496 Eccles JC, Kostyuk PG, Schmidt RF (1962) Central pathways responsible for depolarization of primary
497 afferent fibres. J Physiol 161:237-257.

498 Eguibar JR, Quevedo J, Jimenez I, Rudomin P (1994) Selective cortical control of information flow
499 through different intraspinal collaterals of the same muscle afferent fiber. Brain Res 643:328-
500 333.
501 Esposito MS, Capelli P, Arber S (2014) Brainstem nucleus MdV mediates skilled forelimb motor tasks.
502 Nature 508:351-356.
503 Fink AJ, Croce KR, Huang ZJ, Abbott LF, Jessell TM, Azim E (2014) Presynaptic inhibition of spinal
504 sensory feedback ensures smooth movement. Nature 509:43-48.
505 Galinanes GL, Bonardi C, Huber D (2018) Directional Reaching for Water as a Cortex-Dependent
506 Behavioral Framework for Mice. Cell Rep 22:2767-2783.
507 Gunaydin LA, Yizhar O, Berndt A, Sohal VS, Deisseroth K, Hegemann P (2010) Ultrafast optogenetic
508 control. Nat Neurosci 13:387-392.
509 Guo JZ, Graves AR, Guo WW, Zheng J, Lee A, Rodriguez-Gonzalez J, Li N, Macklin JJ, Phillips JW,
510 Mensh BD, Branson K, Hantman AW (2015) Cortex commands the performance of skilled
511 movement. Elife 4:e10774.
512 Hantman AW, Jessell TM (2010) Clarke's column neurons as the focus of a corticospinal corollary
513 circuit. Nat Neurosci 13:1233-1239.
514 Hochman S, Shreckengost J, Kimura H, Quevedo J (2010) Presynaptic inhibition of primary afferents
515 by depolarization: observations supporting nontraditional mechanisms. Ann N Y Acad Sci
516 1198:140-152.
517 Hughes DI, Mackie M, Nagy GG, Riddell JS, Maxwell DJ, Szabo G, Erdelyi F, Veress G, Szucs P, Antal M,
518 Todd AJ (2005) P boutons in lamina IX of the rodent spinal cord express high levels of
519 glutamic acid decarboxylase-65 and originate from cells in deep medial dorsal horn. Proc Natl
520 Acad Sci U S A 102:9038-9043.
521 Kamiyama T, Kameda H, Murabe N, Fukuda S, Yoshioka N, Mizukami H, Ozawa K, Sakurai M (2015)
522 Corticospinal tract development and spinal cord innervation differ between cervical and
523 lumbar targets. J Neurosci 35:1181-1191.

524 Karadimas SK, Satkunendrarajah K, Laliberte AM, Ringuette D, Weisspapir I, Li L, Gosgnach S, Fehlings
525 MG (2019) Sensory cortical control of movement. Nat Neurosci.
526 Kirkcaldie M, Watson c, Paxinos G, Franklin K (2012) Straightening out the mouse neocortex. In:
527 Australian Neuroscience Society Annual Conference. Goald Coast, QLD.
528 Lavoie S, Drew T (2002) Discharge characteristics of neurons in the red nucleus during voluntary gait
529 modifications: a comparison with the motor cortex. J Neurophysiol 88:1791-1814.
530 Lemon RN (2008) Descending pathways in motor control. Annu Rev Neurosci 31:195-218.
531 Li CX, Waters RS (1991) Organization of the mouse motor cortex studied by retrograde tracing and
532 intracortical microstimulation (ICMS) mapping. Can J Neurol Sci 18:28-38.
533 Libbrecht S, Van den Haute C, Malinouskaya L, Gijsbers R, Baekelandt V (2017) Evaluation of WGA-
534 Cre-dependent topological transgene expression in the rodent brain. Brain Struct Funct
535 222:717-733.
536 Liu Y, Latremoliere A, Li X, Zhang Z, Chen M, Wang X, Fang C, Zhu J, Alexandre C, Gao Z, Chen B, Ding
537 X, Zhou JY, Zhang Y, Chen C, Wang KH, Woolf CJ, He Z (2018) Touch and tactile neuropathic
538 pain sensitivity are set by corticospinal projections. Nature 561:547-550.
539 Lopez-Bendito G, Sturgess K, Erdelyi F, Szabo G, Molnar Z, Paulsen O (2004) Preferential origin and
540 layer destination of GAD65-GFP cortical interneurons. Cereb Cortex 14:1122-1133.
541 Lorenzo LE, Ramien M, St Louis M, De Koninck Y, Ribeiro-da-Silva A (2008) Postnatal changes in the
542 Rexed lamination and markers of nociceptive afferents in the superficial dorsal horn of the
543 rat. JComp Neurol 508:592-604.
544 Mao T, Kusefoglu D, Hooks BM, Huber D, Petreanu L, Svoboda K (2011) Long-range neuronal circuits
545 underlying the interaction between sensory and motor cortex. Neuron 72:111-123.
546 McComas AJ (2016) Hypothesis: Hughlings Jackson and presynaptic inhibition: is there a big picture? J
547 Neurophysiol 116:41-50.
548 Mesnage B, Gaillard S, Godin A, Rodeau JL, Hammer M, von Engelhardt J, Wiseman P, De Koninck Y,
549 Schlichter R, Cordero-Erausquin M (2011) Morphological and functional characterization of

550 cholinergic interneurons of the dorsal horn of the mouse spinal cord. J Comp Neurol
551 519:3139-3158.
552 Miller S, Van Der Burg J, Van Der Meche F (1975) Coordination of movements of the hindlimbs and
553 forelimbs in different forms of locomotion in normal and decerebrate cats. Brain Res 91:217-
554 237.
555 Miri A, Warriner CL, Seely JS, Elsayed GF, Cunningham JP, Churchland MM, Jessell TM (2017)
556 Behaviorally Selective Engagement of Short-Latency Effector Pathways by Motor Cortex.
557 Neuron 95:683-696 e611.
558 Moreno-Lopez Y, Olivares-Moreno R, Cordero-Erausquin M, Rojas-Piloni G (2016) Sensorimotor
559 Integration by Corticospinal System. Front Neuroanat 10:24.
560 Nathan PW, Smith M, Deacon P (1996) Vestibulospinal, reticulospinal and descending propriospinal
561 nerve fibres in man. Brain 119 (Pt 6):1809-1833.
562 Ni Y, Nawabi H, Liu X, Yang L, Miyamichi K, Tedeschi A, Xu B, Wall NR, Callaway EM, He Z (2014)
563 Characterization of long descending premotor propriospinal neurons in the spinal cord. J
564 Neurosci 34:9404-9417.
565 Olivares-Moreno R, Moreno-Lopez Y, Concha L, Martinez-Lorenzana G, Condes-Lara M, Cordero-
566 Erausquin M, Rojas-Piloni G (2017) The rat corticospinal system is functionally and
567 anatomically segregated. Brain Struct Funct 222:3945-3958.
568 Pawlowski SA, Gaillard S, Ghorayeb I, Ribeiro-da-Silva A, Schlichter R, Cordero-Erausquin M (2013) A
569 novel population of cholinergic neurons in the macaque spinal dorsal horn of potential
570 clinical relevance for pain therapy. J Neurosci 33:3727-3737.
571 Prescott SA, De Koninck Y (2003) Gain control of firing rate by shunting inhibition: roles of synaptic
572 noise and dendritic saturation. Proc Natl Acad Sci U S A 100:2076-2081.
573 Reed WR, Shum-Siu A, Onifer SM, Magnuson DS (2006) Inter-enlargement pathways in the
574 ventrolateral funiculus of the adult rat spinal cord. Neuroscience 142:1195-1207.

575 Reed WR, Shum-Siu A, Whelan A, Onifer SM, Magnuson DS (2009) Anterograde labeling of
576 ventrolateral funiculus pathways with spinal enlargement connections in the adult rat spinal
577 cord. Brain Res 1302:76-84.
578 Ribeiro-da-Silva A, Cuello AC (1990) Choline acetyltransferase-immunoreactive profiles are
579 presynaptic to primary sensory fibers in the rat superficial dorsal horn. J Comp Neurol
580 295:370-384.
581 Rudomin P, Schmidt RF (1999) Presynaptic inhibition in the vertebrate spinal cord revisited. Exp Brain
582 Res 129:1-37.
583 Rudomin P, Solodkin M, Jimenez I (1986) PAD and PAH response patterns of group Ia- and Ib-fibers to
584 cutaneous and descending inputs in the cat spinal cord. J Neurophysiol 56:987-1006.
585 Seki K, Fetz EE (2012) Gating of sensory input at spinal and cortical levels during preparation and
586 execution of voluntary movement. J Neurosci 32:890-902.
587 Seki K, Perlmutter SI, Fetz EE (2003) Sensory input to primate spinal cord is presynaptically inhibited
588 during voluntary movement. Nat Neurosci 6:1309-1316.
589 Seki K, Perlmutter SI, Fetz EE (2009) Task-dependent modulation of primary afferent depolarization
590 in cervical spinal cord of monkeys performing an instructed delay task. J Neurophysiol
591 102:85-99.
592 Starkey ML, Barritt AW, Yip PK, Davies M, Hamers FP, McMahon SB, Bradbury EJ (2005) Assessing
593 behavioural function following a pyramidotomy lesion of the corticospinal tract in adult mice.
594 Exp Neurol 195:524-539.
595 Tappe A, Klugmann M, Luo C, Hirlinger D, Agarwal N, Benrath J, Ehrengruber MU, During MJ, Kuner R
596 (2006) Synaptic scaffolding protein Homer1a protects against chronic inflammatory pain. Nat
597 Med 12:677-681.
598 Tennant KA, Adkins DL, Donlan NA, Asay AL, Thomas N, Kleim JA, Jones TA (2011) The organization of
599 the forelimb representation of the C57BL/6 mouse motor cortex as defined by intracortical
600 microstimulation and cytoarchitecture. Cereb Cortex 21:865-876.

601 Tjolsen A, Berge OG, Hunskaar S, Rosland JH, Hole K (1992) The formalin test: an evaluation of the
602 method. Pain 51:5-17.
603 Ueno M, Hayano Y, Nakagawa H, Yamashita T (2012) Intraspinal rewiring of the corticospinal tract
604 requires target-derived brain-derived neurotrophic factor and compensates lost function
605 after brain injury. Brain 135:1253-1267.
606 Ueno M, Nakamura Y, Li J, Gu Z, Niehaus J, Maezawa M, Crone SA, Goulding M, Baccei ML, Yoshida Y
607 (2018) Corticospinal Circuits from the Sensory and Motor Cortices Differentially Regulate
608 Skilled Movements through Distinct Spinal Interneurons. Cell Rep 23:1286-1300 e1287.
609 von Engelhardt J, Eliava M, Meyer AH, Rozov A, Monyer H (2007) Functional characterization of
610 intrinsic cholinergic interneurons in the cortex. JNeurosci 27:5633-5642.
611 Wall PD, Lidierth M (1997) Five sources of a dorsal root potential: their interactions and origins in the
612 superficial dorsal horn. J Neurophysiol 78:860-871.
613 Wang X, Liu Y, Li X, Zhang Z, Yang H, Zhang Y, Williams PR, Alwahab NSA, Kapur K, Yu B, Chen M, Ding
614 H, Gerfen CR, Wang KH, He Z (2017) Deconstruction of Corticospinal Circuits for Goal-
615 Directed Motor Skills. Cell 171:440-455 e414.
616 Zelenin PV, Beloozerova IN, Sirota MG, Orlovsky GN, Deliagina TG (2010) Activity of red nucleus
617 neurons in the cat during postural corrections. J Neurosci 30:14533-14542.

Figure Legends

Figure 1. The same cortical area evokes dorsal root potentials and muscular contractions of the hindlimbs.

A. Schematic experimental design for cortically-evoked (Cx-) DRP and EMG recordings elicited by photostimulation of the contralateral sensorimotor cortex of Thy1::ChR2 mice. DRPs correspond to the presynaptic depolarization of primary afferents propagating antidromically to the suction recording electrode containing a lumbar dorsal root, while EMGs are recorded in the *TA* muscle.

B. Representative traces of a cortically-evoked DRP (top red trace, average of 30 sweeps) and EMG (bottom blue trace, average of 3 sweeps) after photostimulation (blue window) of the contralateral cortex.

C. *Left,* Heatmaps of the amplitude of the responses of cortically-evoked DRPs (top) and EMGs (bottom) in % or the maximum response. *Right*, Overlap of the two maps (red: DRP, blue: EMG) presented as isopotential contour plots (three color grades corresponding to 37%, 50% and 63% of maximum value). Coordinates of the cortex are expressed in mm and centered on *Bregma*. M1: primary motor cortex, M2: secondary motor cortex, and S1: primary sensory cortex, according to the Paxinos atlas (Kirkcaldie et al., 2012).

D. Schematic experimental design to identify GAD65-expressing neurons amongst corticospinal neurons targets: AAV1-CBA-WGA-CRE was injected in the sensorimotor cortex of TdTomato-flex X GAD65::GFP mice. Analysis of extend of the injection site is presented in Figure 1 – Figure Supplement 1, and of the monosynaptic nature of the transynaptic tracing in Figure 1 - Figure Supplement 2.

E. Photomicrographs (z projection of confocal images) of a GAD65::GFP mouse lumbar dorsal horn (localization of the view indicated in the inset) after transynaptic labeling from the

hindlimb sensorimotor contralateral cortex. A target of the CST (expressing TdTomato after transynaptic transfer of WGA-Cre) also expresses GAD65::GFP. CST: corticospinal tract. Similar experiment in ChAT::EGFP mice is presented in Figure 1 – Figure Supplement 3.

Figure 2. The corticospinal tract is essential for cortically-evoked inhibition of primary afferents.

A. *Left*, diagram showing direct and indirect cortical-to-spinal paths. In green: paths potentially activated by photostimulation in the cortex of Thy1::ChR2 mice. *Right*, experimental design.
B. *Left*, drawing showing the extent of the pyramidal lesion (in grey, pyx) in the frontal plane (distance to *Bregma* indicated) in two animals whose recordings are respectively illustrated in C and D. *Right*, diagram showing the indirect cortical-to-spinal paths spared by the pyramidotomy. Systematic histological analysis of the pyramidotomies is presented in Figure 2 – Figure Supplement 1.
C. *Left*, Representative traces of cortically-evoked DRPs recording before (red) and after (grey) CST lesion (average of 30 traces). *Right*, the pyramidotomy abolishes cortically-evoked DRPs (p= 0.006, one-way ANOVA, n= 3 mice). Post-hoc test Holm-Sidak, *P < 0.05
D. *Left*, Representative traces of cortically-evoked EMG recording before (blue) and after (grey) pyramidal lesion (average of 3 traces). *Right*, There is no significant change in the S/N ratio of the EMG response before and after the pyramidal lesion (p=0.517, one-way ANOVA, n= 4 mice). Grey zone: noise level (see Methods). EMG Z-scores for individual mice before and after pyramidotomy are presented in Figure 2 – Figure Supplement 2.

Figure 3. The corticospinal tract can encode muscular contractions.

A. *Left*, diagram illustrating corticospinal neurons and their collaterals expressing ChR2 after retrograde infection in the lumbar cord with a retroAAV. *Right*, experimental design: the photostimulation and EMG recording session took place at least 3 weeks after the infection.

B. Sagittal image from the sensorimotor cortex (Lateral= 0.68 mm), showing retrogradely labeled corticospinal neurons (expressing ChR2-TdTomato fluorescence).

C. Drawing of a cortex top view, showing the localization of retrogradely labeled corticospinal neurons in the 5 animals (solid lines). They are within the area functionally determined as inducing DRPs and EMGs in the hindlimb (dashed lines).

D. *Left*, drawing showing the extent of the pyramidal lesion in the animal whose recordings are illustrated in E. *Right*, diagram showing the supraspinal collaterals of ChR2-expressing CS neurons spared by the pyramidotomy. Systematic histological analysis of the pyramidotomies is presented in Figure 2 – Figure Supplement 1.

E. *Left*, cortically evoked EMG recordings before (blue) and after (grey) the pyramidal lesion. *Right,* the pyramidotomy abolishes cortically-evoked EMG (p=0.012, one-way ANOVA, n= 5 mice). Post-hoc test Holm-Sidak, *P < 0.05. Grey zone: noise level (see Methods). EMG Z-scores for individual mice before and after pyramidotomy are presented in Figure 2 – Figure Supplement 2.

The blue window on recording traces indicates light stimulation. SMC: sensorimotor cortex, BSMN: brain stem motor nuclei, C-Th: cervico-thoracic spinal cord, L-SC: Lumbo-sacral spinal cord.

Figure 4. Lumbar corticospinal postsynaptic neurons encode DRPs but no movements.

A. Experimental design: the targets of the CST are labeled through a transynaptic approach consisting of AAV1-CBA-WGA-CRE injection in the hindlimb sensorimotor cortex of TdTomato-flex mice.

B. Localization of the spinal targets of the CST: heatmap showing the distribution of the neurons in the lumbar cord (6 mm long) projected into the transverse plane (average of 9 mice) (*left*) or horizontal plane (average of 6 mice) (*right*) plane.

C. *Left*, Diagram illustrating that only lumbar direct targets of the CST express CHETA in the following experiment. *Right*, Experimental design: TdTomato-flex mice received an injection of AAV1-CBA-WGA-CRE in the hindlimb sensorimotor cortex and an injection of AAV1-Efl-flex-CHETA-eYFP in the L4 spinal segment.

D. Photomicrographs (z projection of confocal images) from the dorsal horn of the spinal cord (laminae V/VI); the arrows point at two targets of the CST expressing TdTomato+ and CHETA-eYFP.

E. Experimental design illustrating spinal photostimulation of the lumbar targets of the CST.

F. Representative traces of DRP (red trace, average of 60 traces) and EMG (blue trace, average of 3 traces) recordings from the same animal after photostimulation of the lumbar targets of the CST (blue window).

G. Photostimulation of the lumbar targets of the CST induces DRPs (left) but no EMG signal (right). Grey zone: noise level (see Methods). EMG Z-scores for individual mice are presented in Figure 2 – Figure Supplement 2.

SMC: sensorimotor cortex, BSMN: brain stem motor nuclei, C-Th: cervico-thoracic spinal cord, L-SC:Lumbo-sacral spinal cord.

710 **Figure Supplement material:**

711 Figure 1 - Figure Supplement 1. Sensorimotor injection site analyses : cortical layer V fluorescence
712 quantification.

713 Figure 1 - Figure Supplement 2. Monosynaptic transynaptic tracing from the cortex

714 Figure 1 - Figure Supplement 3. Postsynaptic corticospinal neurons do not colocalize with ChAT.

715 Figure 2 - Figure Supplement 1. Histology of the pyramidotomies.

716 Figure 2 Figure Supplement 2. Z-score of individual EMG responses assessing the significance of the
717 corresponding S/N ratio

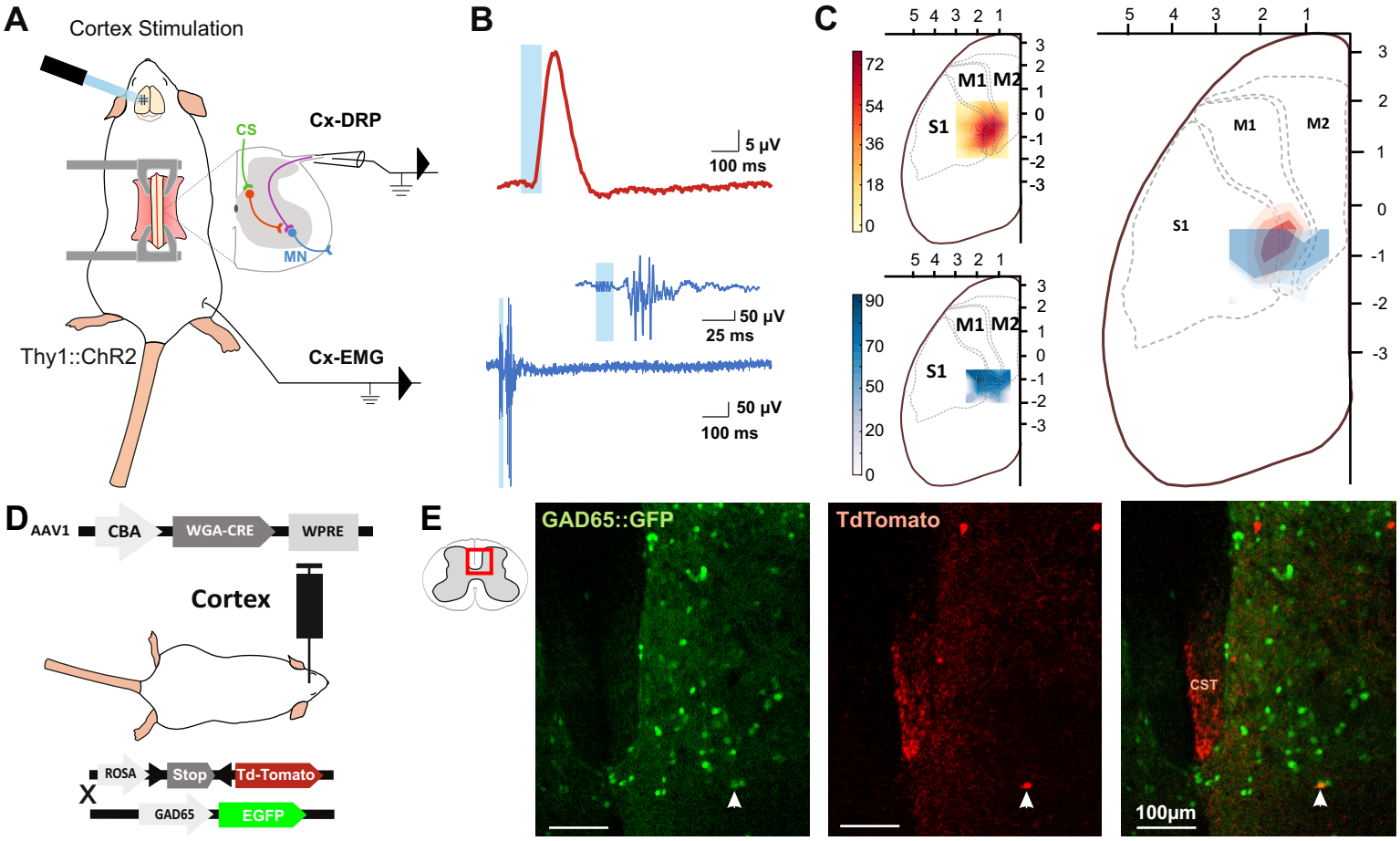

Figure 1. The same cortical area evokes dorsal root potentials and muscular contractions of the hindlimbs.

A. Schematic experimental design for cortically-evoked (Cx-) DRP and EMG recordings elicited by photostimulation of the contralateral sensorimotor cortex of Thy1::ChR2 mice. DRPs correspond to the presynaptic depolarization of primary afferents propagating antidromically to the suction recording electrode containing a lumbar dorsal root, while EMGs are recorded in the *TA* muscle.

B. Representative traces of a cortically-evoked DRP (top red trace, average of 30 sweeps) and EMG (bottom blue trace, average of 3 sweeps) after photostimulation (blue window) of the contralateral cortex.

C. *Left,* Heatmaps of the amplitude of the responses of cortically-evoked DRPs (top) and EMGs (bottom) in % or the maximum response. *Right*, Overlap of the two maps (red: DRP, blue: EMG) presented as isopotential contour plots (three color grades corresponding to 37%, 50% and 63% of maximum value). Coordinates of the cortex are expressed in mm and centered on *Bregma*. M1: primary motor cortex, M2: secondary motor cortex, and S1: primary sensory cortex, according to the Paxinos atlas (Kirkcaldie et al., 2012).

D. Schematic experimental design to identify GAD65-expressing neurons amongst corticospinal neurons targets: AAV1-CBA-WGA-CRE was injected in the sensorimotor cortex of TdTomato-flex X GAD65::GFP mice. Analysis of extend of the injection site is presented in Figure 1 – Figure Supplement. 1, and of the monosynaptic nature of the transynaptic tracing in Figure 1 - Figure Supplement 2.

E. Photomicrographs (z projection of confocal images) of a GAD65::GFP mouse lumbar dorsal horn (localization of the view indicated in the inset) after transynaptic labeling from the hindlimb sensorimotor contralateral cortex. A target of the CST (expressing TdTomato after transynaptic transfer of WGA-Cre) also expresses GAD65::GFP. CST: corticospinal tract. Similar experiment in ChAT::EGFP mice is presented in Figure 1 – Figure Supplement 3.

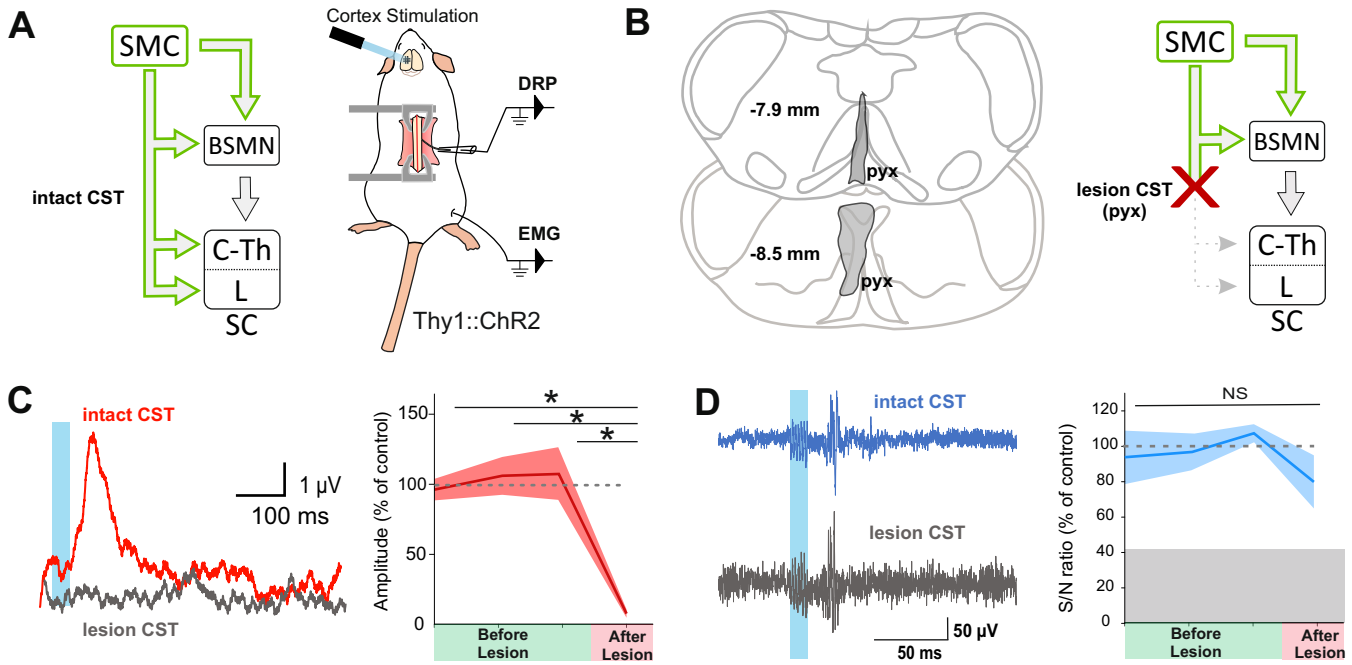

Figure 2. The corticospinal tract is essential for cortically-evoked inhibition of primary afferents.

A. *Left*, diagram showing direct and indirect cortical-to-spinal paths. In green: paths potentially activated by photostimulation in the cortex of Thy1::ChR2 mice. *Right*, experimental design.

B. *Left*, drawing showing the extent of the pyramidal lesion (in grey, pyx) in the frontal plane (distance to *Bregma* indicated) in two animals whose recordings are respectively illustrated in C and D. *Right*, diagram showing the indirect cortical-to-spinal paths spared by the pyramidotomy. Systematic histological analysis of the pyramidotomies is presented in Figure 2 – Figure Supplement 1.

C. *Left*, Representative traces of cortically-evoked DRPs recording before (red) and after (grey) CST lesion (average of 30 traces). *Right*, the pyramidotomy abolishes cortically-evoked DRPs ($p = 0.006$, one-way ANOVA, n= 3 mice). Post-hoc test Holm-Sidak, $*P < 0.05$

D. *Left*, Representative traces of cortically-evoked EMG recording before (blue) and after (grey) pyramidal lesion (average of 3 traces). *Right*, There is no significant change in the S/N ratio of the EMG response before and after the pyramidal lesion ($p=0.517$, one-way ANOVA, n= 4 mice). Grey zone: noise level (see Methods). EMG Z-scores for individual mice before and after pyramidotomy are presented in Figure 2 – Figure Supplement 2.

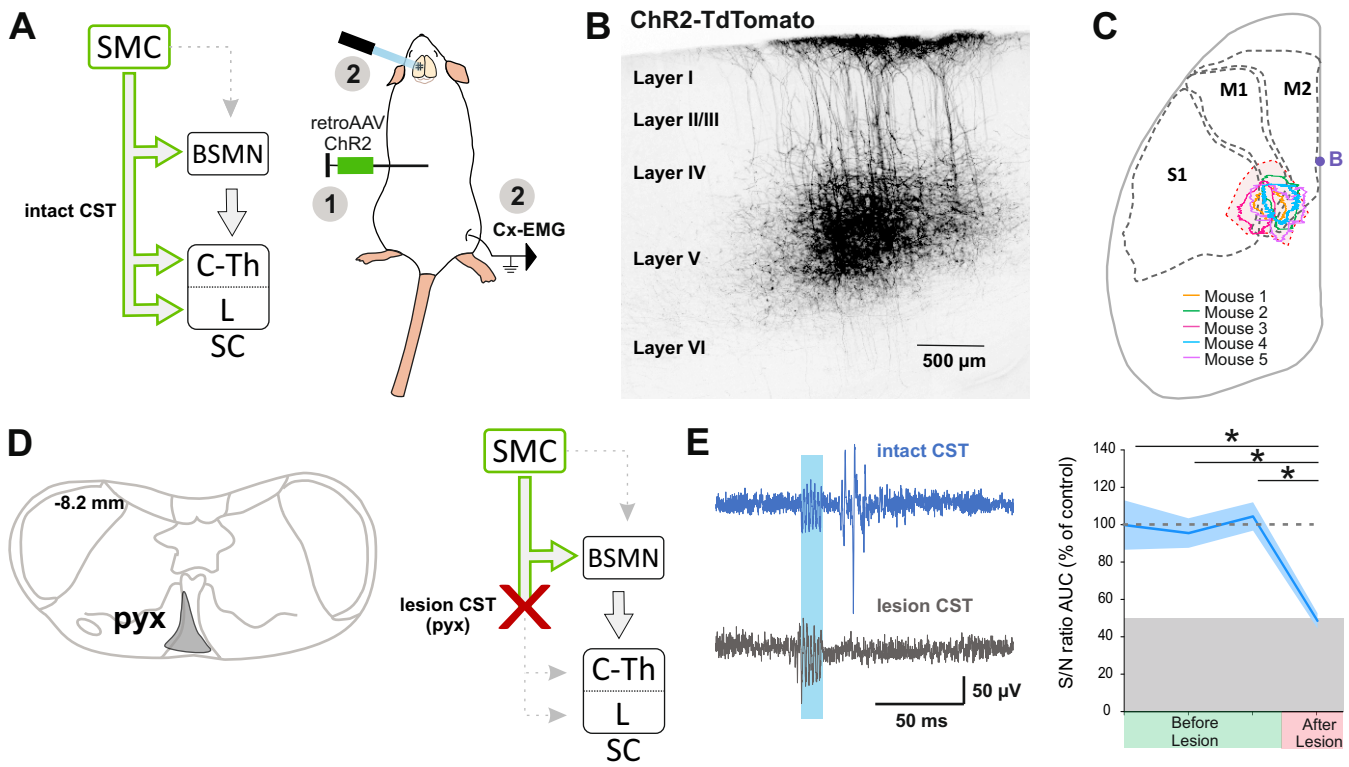

Figure 3. The corticospinal tract can encode muscular contractions.

A. *Left*, diagram illustrating corticospinal neurons and their collaterals expressing ChR2 after retrograde infection in the lumbar cord with a retroAAV. *Right*, experimental design: the photostimulation and EMG recording session took place at least 3 weeks after the infection.

B. Sagittal image from the sensorimotor cortex (Lateral= 0.68 mm), showing retrogradely labeled corticospinal neurons (expressing ChR2-TdTomato fluorescence).

C. Drawing of a cortex top view, showing the localization of retrogradely labeled corticospinal neurons in the 5 animals (solid lines). They are within the area functionally determined as inducing DRPs and EMGs in the hindlimb (dashed lines).

D. *Left*, drawing showing the extent of the pyramidal lesion in the animal whose recordings are illustrated in E. *Right*, diagram showing the supraspinal collaterals of ChR2-expressing CS neurons spared by the pyramidotomy. Systematic histological analysis of the pyramidotomies is presented in Figure 2 – Figure Supplement 1.

E. *Left*, cortically evoked EMG recordings before (blue) and after (grey) the pyramidal lesion. *Right,* the pyramidotomy abolishes cortically-evoked EMG ($p=0.012$, one-way ANOVA, n= 5 mice). Post-hoc test Holm-Sidak, $*P < 0.05$. Grey zone: noise level (see Methods). EMG Z-scores for individual mice before and after pyramidotomy are presented in Figure 2 – Figure Supplement 2.

The blue window on recording traces indicates light stimulation. SMC: sensorimotor cortex, BSMN: brain stem motor nuclei, C-Th: cervico-thoracic spinal cord, L-SC: Lumbo-sacral spinal cord.

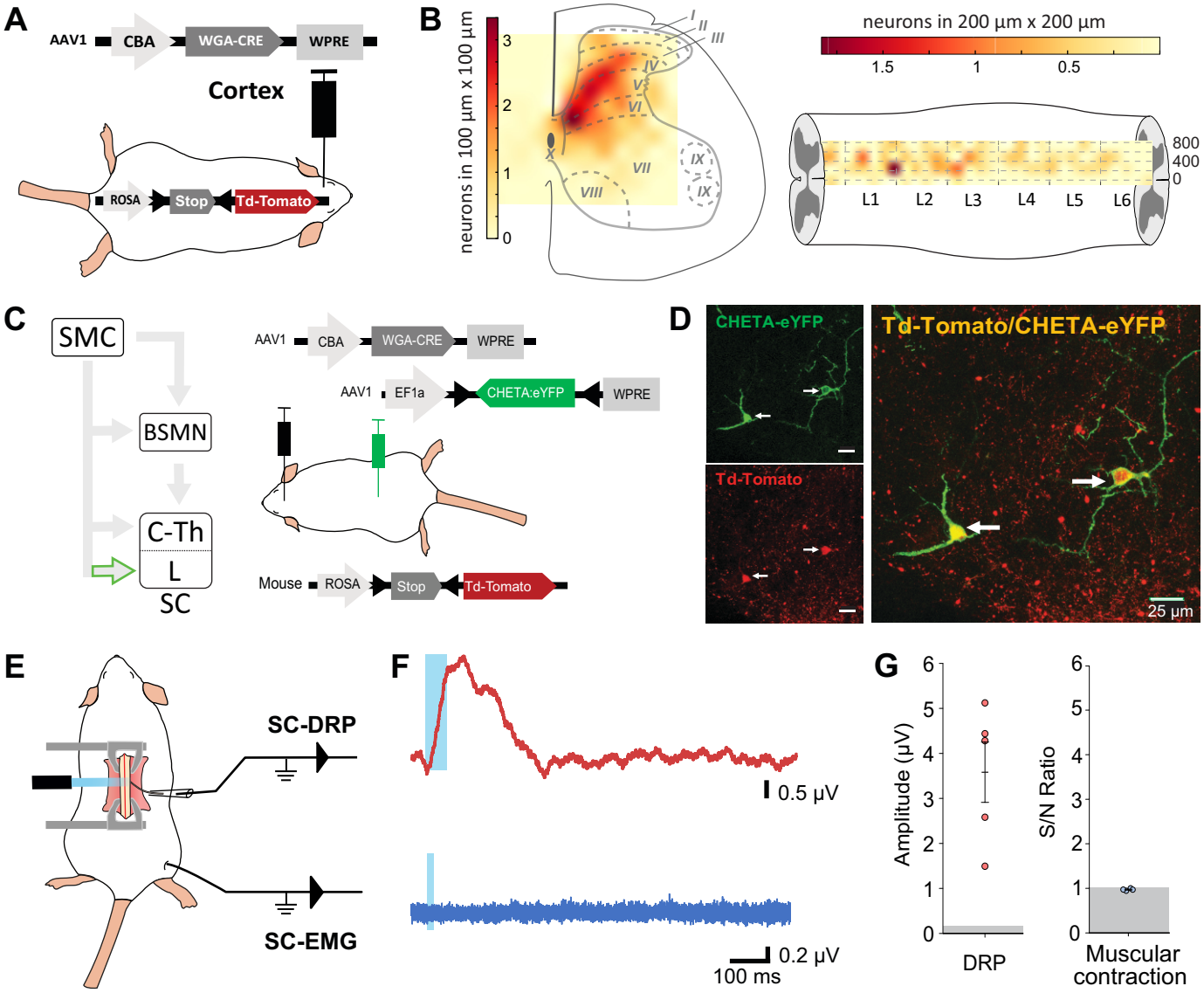

Figure 4. Lumbar corticospinal postsynaptic neurons encode DRPs but no movements.

A. Experimental design: the targets of the CST are labeled through a transynaptic approach consisting of AAV1-CBA-WGA-CRE injection in the hindlimb sensorimotor cortex of TdTomato-flex mice.

B. Localization of the spinal targets of the CST: heatmap showing the distribution of the neurons in the lumbar cord (6 mm long) projected into the transverse plane (average of 9 mice) (*left*) or horizontal plane (average of 6 mice) (*right*) plane.

C. *Left*, Diagram illustrating that only lumbar direct targets of the CST express CHETA in the following experiment. *Right*, Experimental design: TdTomato-flex mice received an injection of AAV1-CBA-WGA-CRE in the hindlimb sensorimotor cortex and an injection of AAV1-Efl-flex-CHETA-eYFP in the L4 spinal segment.

D. Photomicrographs (z projection of confocal images) from the dorsal horn of the spinal cord (laminae V/VI); the arrows point at two targets of the CST expressing TdTomato+ and CHETA-eYFP.

E. Experimental design illustrating spinal photostimulation of the lumbar targets of the CST.

F. Representative traces of DRP (red trace, average of 60 traces) and EMG (blue trace, average of 3 traces) recordings from the same animal after photostimulation of the lumbar targets of the CST (blue window).

G. Photostimulation of the lumbar targets of the CST induces DRPs (left) but no EMG signal (right). Grey zone: noise level (see Methods). EMG Z-scores for individual mice are presented in Figure 2 – Figure Supplement 2.

SMC: sensorimotor cortex, BSMN: brain stem motor nuclei, C-Th: cervico-thoracic spinal cord, L-SC:Lumbo-sacral spinal cord.